





Synthesis of Carbon and Gold Nanoparticles in Ionic Liquid Crystals: Structural Properties and Electrical Behavior for Electro-Optical Sensors

Dmytro Zhulai^{1,2} | Nazariy Boichuk¹ | Denys Pustovyi¹ | Oleksandr Kovalchuk^{2,3} | Yuriy Garbovskiy⁴ | Gertruda Klimusheva² | Tatyana Mirnaya⁵ | Galina Yaremchuk⁵ | Svetlana Vitusevich¹

¹Forschungszentrum Jülich, Institute of Biological Information Processing (IBI-3), Jülich, Germany | ²Department of Physics of Crystals, Institute of Physics of NAS of Ukraine, Kyiv, Ukraine | ³Department of Applied Physics and Higher Mathematics, Kyiv National University of Technologies and Design, Kyiv, Ukraine | ⁴Department of Physics and Engineering Physics, Central Connecticut State University, New Britain, Connecticut, USA | ⁵Department of Physical and Inorganic Chemistry, V.I. Vernadsky Institute of General and Inorganic Chemistry of NAS of Ukraine, Kyiv, Ukraine

Correspondence: Svetlana Vitusevich (s.vitusevich@fz-juelich.de)

Received: 3 April 2024 | Revised: 6 August 2024 | Accepted: 12 August 2024

Funding: D. Zhulai greatly appreciates a research grant from the German National Academy of Sciences Leopoldina. Y. Garbovskiy would like to acknowledge funding from the CSU—AAUP Faculty Research Grant and the NASA CT Space Grant. The authors acknowledge funding from NASU via the project No.

Keywords: carbon and gold nanoparticles | dielectric properties | ionic liquid crystals | nanocomposites | TEM and SEM images

ABSTRACT

The structural and electrical properties of ionic metal-alkanoate nanocomposites obtained based on a cadmium octanoate matrix with individual carbon and gold nanoparticles (NPs) as well as their combination are studied. Carbon and gold NPs were chemically synthesized within the smectic A phase of $Cd^{+2}(C_7H_{15}COO^-)_2$, which served as a well-ordered nanoreactor. Scanning electron microscopy (SEM) and transmission electron microscopy (TEM) data provide information on NPs location and allow the estimation of the sizes of the synthesized NPs inside the glassy liquid crystalline matrix. It is shown that the size and shape of the NPs were precisely controlled during synthesis, resulting in highly stable and organized nanocomposites. The electrical characteristics were studied in a wide temperature range corresponding to different phase states of the nanocomposites. We compared the electrical properties of both pure matrix and nanocomposites with carbon and gold NPs to identify the potential of the nanocomposite materials for designing new sensor structures. Notably, the nanocomposites exhibited anisotropic conductivity, highlighting the structural anisotropy of the material. In addition, using NPs allows fine-tuning of the electrical properties of a metal-alkanoate host matrix. The obtained nanocomposites open prospects for the development of electro-optical sensors with high sensitivity and specificity that can be used to detect a variety of chemical and physical parameters including temperature, composition of substances, and environment.

1 | Introduction

Studies of materials with new unique properties that could provide breakthroughs in various scientific fields represent the main challenges of science and technology. Nanocomposites have attracted particular interest due to their unique compositiondetermined properties. These materials, which combine nanosized particles or structures in a matrix of another material, are opening up new horizons in many fields, ranging from electronics [1–4] to medicine [5–10]. Their potential for optimizing mechanical, electrical, and optical properties is particularly valuable. In this context, one of the key directions in the development

This is an open access article under the terms of the Creative Commons Attribution License, which permits use, distribution and reproduction in any medium, provided the original work is properly cited.

© 2025 The Author(s). Nano Select published by Wiley-VCH GmbH.

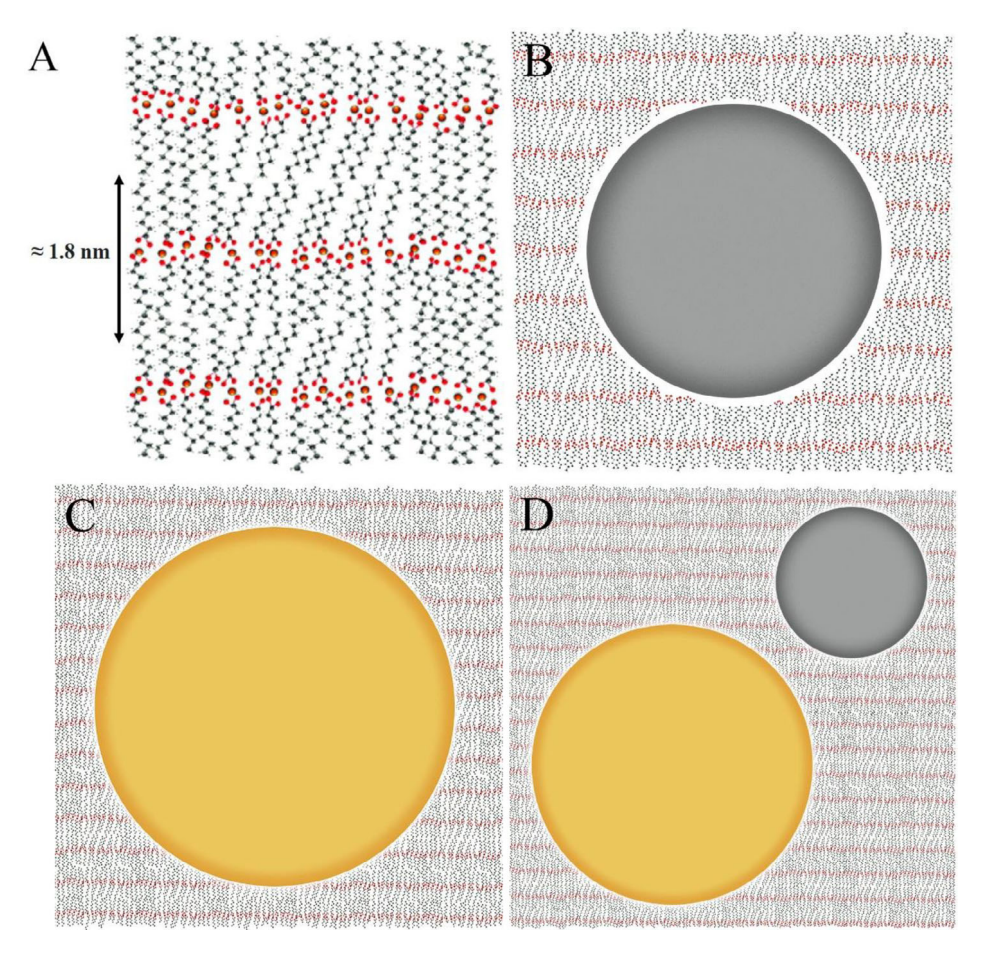


FIGURE 1 | Schematic presentation of LC materials with characteristic relations at the nanoscale. (A) Sizes between layers matrix CdC_8 . (B) Sizes of C NPs synthesized in a CdC_8 matrix. (C) Sizes Au NPs synthesized in a CdC_8 matrix.

of nanocomposite technology is the synthesis of nanoparticles (NPs) directly in the matrix [11–16]. This approach demonstrates several advantages, including the ability to closely control the size, shape, and distribution of NPs [17]. This prevents agglomeration and ensures the stability and durability of composites, making them even more attractive for practical applications. Particular attention is paid to composite materials consisting of ionic liquid crystals (LCs) [18-22] and different types of NPs. These composites have several unique characteristics that can be used in optoelectronics, photonics, and other fields. In [23], the structural characteristics were investigated of various types of NPs synthesized in the mesomorphic metal alkanoates matrix. The possibility of synthesizing core-shell NPs was also confirmed. In several studies [24-26], the optical nonlinearities of glass nanocomposites of mesogenic metal alkanoates with bimetallic NPs were studied. In addition, the importance and relevance of studying the LCs' photovoltaic and photoconductive properties were emphasized in [27, 28]. The analysis of new composite materials and their properties could lead to discovery of new methods and technologies in optoelectronics and other related fields.

In this work, we analyze the main characteristics of new nanocomposites, fabricated based on cadmium octanoate with individual carbon (C) and gold (Au) NPs as well as their combination. We identify the properties of nanocomposites using several methods, including transmission electron microscopy

(TEM), scanning electron microscopy (SEM) and impedance spectroscopy. These studies provide new insights into the role of C and Au NPs in the electrical performance of these materials. In addition, we also analyze the effect of both C and Au NPs (i.e., ionic LCs are doped with both C and Au nanodopants) on the electrical properties of ionic LCs. The results open prospects for the development of new, highly efficient devices based on such advanced nanocomposite materials.

2 | Materials Preparation

New nanocomposites with individual C and Au NPs as well as their combination are fabricated based on cadmium octanoate: $Cd^{+2}(C_7H_{15}COO^-)_2$, abbreviated as CdC_8 , matrix. It is known, that metal-alkanoates demonstrate thermo-mesomorph properties [29], allowing the formation of ionic LCs. When the crystal is heated to its melting temperature and when the isotropic melt is cooled to its mesophase brightening temperature, some bivalent metal-alkanoates, including CdC_8 can form glasses with smectic ordering. Cadmium octanoate melts at 98°C and forms a smectic A mesophase within temperatures ranging from 98°C to 165°C. During the cooling process, the mesophase of cadmium octanoate does not crystallize. Instead, a glass state is formed with a bilayer distance of 1.8 nm (Figure 1A) [30] due to the supercooling state of the material. It should be noted, that CdC_8 is used as a matrix due to its unique properties, including mesophase state

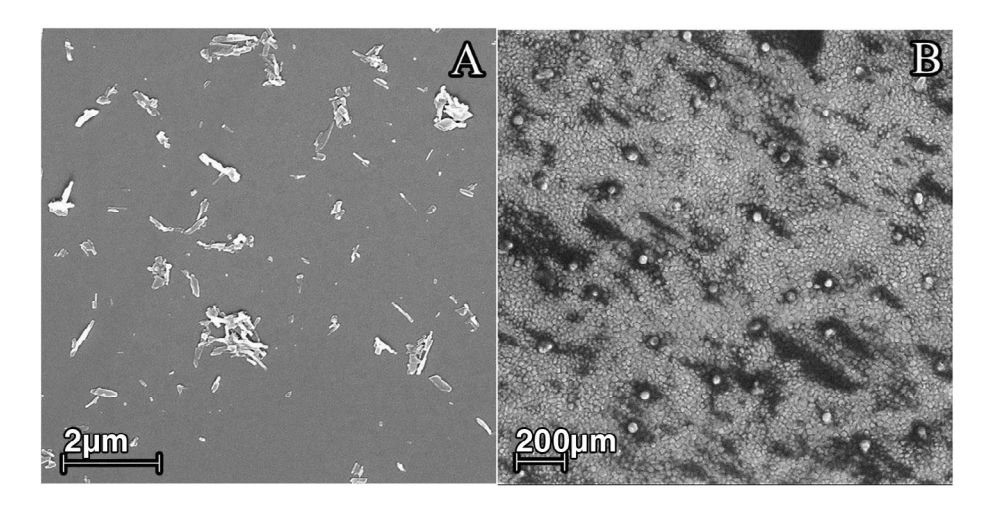


FIGURE 2 (A) SEM image of matrix CdC₈ on top of the ITO glass. (B) SEM image of Au NPs on top of the ITO glass.

in a wide temperature range of 98°C–165°C, which provides a stable environment for nanoparticle synthesis. Unlike matrices based on Pb or Zn, CdC₈ has higher temperature stability and improved glass-forming properties. The important advantage of the cadmium octanoate mesophase is also following. Smectic A mesophase is working as a nanoreactor for the syntheses of nanocomposite materials with metal and semiconductor NPs.

To prepare a nanocomposite based on an LC CdC₈ matrix with C NPs, an aqueous solution containing 2 wt% C NPs was added to CdC₈ powder. The C NPs were synthesized using an autoclave hydrothermal method [31], with citric acid and ethylenediamine as reagents. It should be noted that for the fabrication of C NPs, high temperatures are currently used. The temperatures are not compatible for C NPs to be synthesized directly in CdC₈ material, therefore the NPs are introduced using their aqueous solution. This avoids the destruction of the liquid crystal structure and allows the integration of C nanoparticles into the matrix without changing its properties. The thoroughly mixed material was melted in an inert argon atmosphere and maintained at 120°C for 15 min. Upon fast cooling of the melt, a glassy nanocomposite of CdC₈ with C NPs was obtained (Figure 1B). During the preparation process, the mixture gradually changes color from colorless to yellow, indicating chemical changes within the matrix and the formation of nanostructured C inclusions.

Au nanoparticles can be synthesized directly in the CdC8 matrix at moderate temperatures, which avoids matrix damage and ensures uniform nanoparticle distribution. Moreover, the synthesis parameters can be adjusted to control the size and morphology of the nanoparticles. The nanocomposite based on an LC CdC₈ matrix with Au NPs was prepared as follows. Au NPs were synthesized in an LC environment using CdC₈ as a template at 120°C in an argon atmosphere. The synthesis process was carried out by chemical reduction of Au³⁺ cations from tetrachloroauric acid (H[AuCl₄]·3H₂O), with the octanoate anion acting as a reducing agent [32]. The final CdC₈ nanocomposite contained approximately 4 mol% Au NPs. The duration of synthesis varied from 1 to 2 h. The resulting LC glass nanocomposites were formed by cooling the CdC₈ LC phase to room temperature with Au NPs inside (Figure 1C). Because of this process, glass-like samples of purple color were obtained. Synthesis directly in the liquid crystal matrix allows obtaining a narrow distribution in size of Au nanoparticles. It should be noted that Au NPs were synthesized directly in the CdC₈ matrix, which allows more flexibility to develop nanocomposites with unique properties.

To prepare a nanocomposite of cadmium octanoate with both C and Au NPs, tetrachloroauric acid (4 mol%) and a solution of C NPs (2 wt%) were added to CdC_8 powder. The resulting material was thoroughly mixed, heated to 120° C in an argon atmosphere and maintained at this temperature for 2 h. During the synthesis, the reaction mixture gradually changed color from a transparent yellowish melt to a rich brown. Upon cooling, the melt solidified into a violet-colored glassy nanocomposite containing both C and Au NPs (Figure 1D). The integration of several types of nanoparticles, such as Au and C into a single matrix opens new ways for the development of new materials with unique properties.

This nanoreactor technology allows the formation of glassy nanocomposite materials with uniformly distributed NPs, characterized by a narrow size distribution within the matrix, as will be shown below.

3 | Structure of Synthesized Nanoparticles

To analyze the samples, we used the SEM LEO 1550 (Zeiss, Oberkochen, Germany) and TEM FEI Titan Tecnai G2 F20, which is equipped with a Gatan Tridiem 863P post-column image filter (GIF) and a high-angle energy dispersive x-ray (EDX) detector. This setup allows for a variety of studies, such as conventional imaging and diffraction, the recording of bright- and dark-field scanning transmission electron microscopy (STEM) images, and the acquisition of elemental maps extracted from energy electron loss spectra (EELS) or EDX signals. To study the sizes of C and Au NPs, we dissolved the nanocomposite CdC₈ + C 2 wt% + Au 4 mol% in hexane— C_6H_{14} . Then dropped 1 μL of the obtained substance onto the top of the indium tin oxide (ITO) glass for SEM analysis and carbon film-supported copper grid for TEM analysis and left these samples under the hood for hexane evaporation. It should be noted that the matrix was not completely dissolved in hexane. Small parts of the matrix were present in the resulting solution (Figure 2A). An SEM image of Au NPs on the surface of ITO glass is shown in Figure 2B. More detailed information

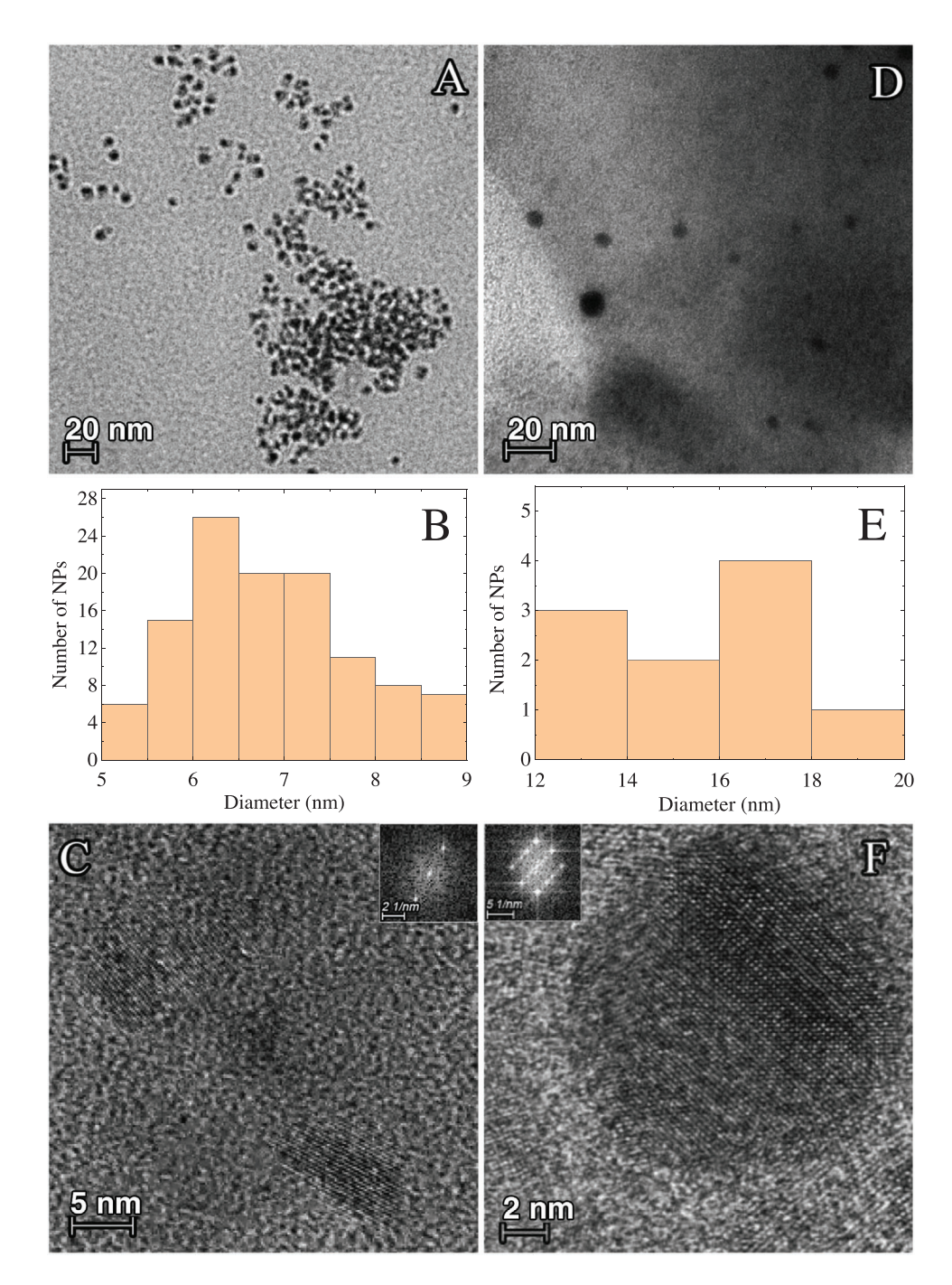


FIGURE 3 \mid (A) TEM image of C NPs without CdC₈ matrix on top of the carbon film. (B) Size distribution of C NPs. (C) TEM image demonstrating the group of C NPs. (D) TEM image of Au NPs in a CdC₈ matrix. (E) size distribution of Au NPs. (F) TEM images reflecting the atomic structure of Au NPs. Inserts in (C) and (F) represent the fast Fourier transform (FFT) of the HRTEM images. The FFT spots correspond to the atomic planes of the sample lattice.

about nanocomposite samples was obtained using the TEM. The results of our SEM and TEM studies show that during the synthesis, the NPs could be observed both in the state when they were outside the matrix (Figure 3A) and inside the matrix (Figure 3B).

For analysis of NPs size based on TEM images, we used the ImageJ software. The image in Figure 3A shows the dimensions and shape of C NPs without CdC_8 matrix on top of the carbon film. The size distribution of the C NPs can be seen, ranging from

about 5 to 9 nm. The main diameter of NPs is in the range of 6–7 nm. The synthesis of C NPs allows to obtain high-quality NPs of a small dispersion in size. TEM images demonstrate that C NPs are spherical.

Figure 3D shows that Au NPs are uniformly distributed in the CdC_8 matrix without sticking or aggregating. Their average diameters are 12–20 nm, and they have a round shape. The main diameters of NPs correspond to the middle of this range, about 15–17 nm. These data show the stability and homogeneity of Au

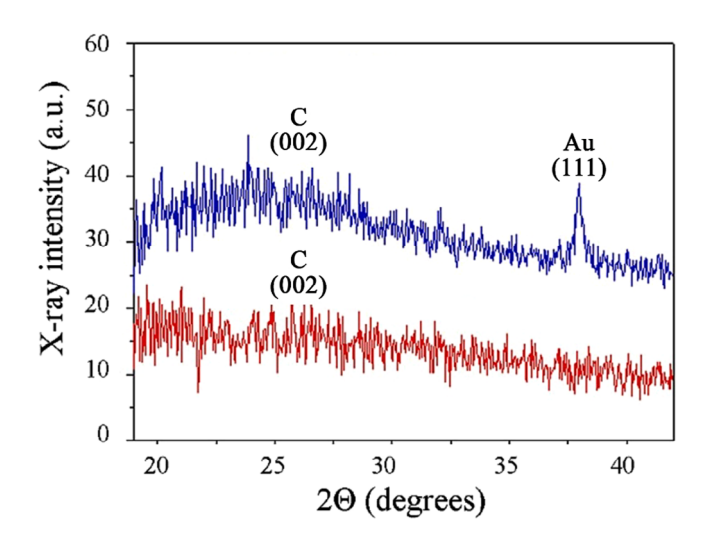


FIGURE 4 | X-ray scattering pattern of nanocomposite materials (Red) $CdC_8 + 2$ wt C NPs; (Blue) $CdC_8 + 2$ wt C + 4 mol Au NPs.

NPs in this system. A small size dispersion was observed, which reflects the good quality of the synthesis of NPs. It should be noted that NPs have a relatively narrow size distribution, which is important for many applications, where uniformity and size stability of NPs are required to achieve certain properties and material functionality.

To obtain data on the atomic structure of the NPs, we performed high-resolution TEM studies. For Au NPs (Figure 3F), we found that they average an interatomic distance of 0.28 nm. At the same time, for C NPs (Figure 3C) the distance is in the range from 0.35 to 0.37 nm. These results further confirm that the developed synthesis process enables the fabrication of C and Au NPs with unique structural characteristics. It should be noted that the size of NPs is the same for individual C and Au NPs as well as in the case of their combination according to our TEM data. This is a significant achievement, which is important for the practical application of nanomaterials in various fields of research and development. The characterization of obtained materials using x-ray diffraction (XRD) method (Figure 4) supports good quality of nanocomposites with C and Au NPs.

The XRD data reflect well-resolved responses corresponding to atoms of C and Au due to introduced Au and C NPs in the CdC_8 matrix.

4 | Dielectric Properties

Since CdC_8 nanocomposites have a layered smectic A structure [33], electrical measurements in different orientations (along and perpendicular to the cation-anion layers) may allow for a deeper understanding of charge transport in these unique systems. In this work, we studied the charge transfer in the direction perpendicular to the cation-anion layers, as is schematically shown in (Figure 5). Arrow in Figure 5 shows the direction of charge transfer. To measure the electrical properties of the pure CdC_8 matrix and this CdC_8 matrix with different types of synthesized C and Au NPs, we used ITO glass slides with sheet resistances ranging from 70 Ω/\Box to 100 Ω/\Box . The preparation

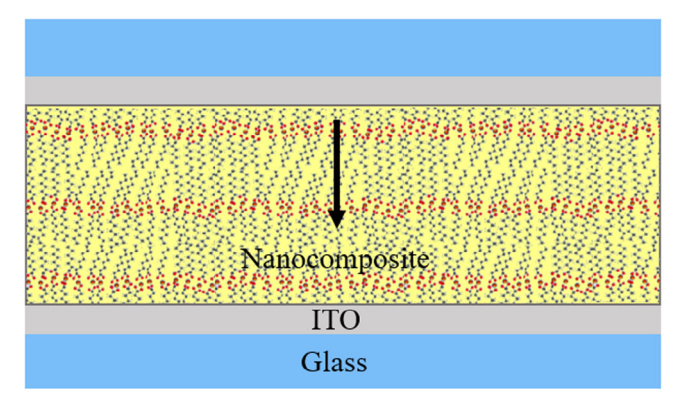


FIGURE 5 | Schematic presentation of nanocomposite sample at applied voltage, reflecting charge transfer perpendicular to the cationanion layers in the CdC_8 nanocomposite. The arrow shows the direction of the charge transfer.

process includes the steps described below. First, two glass slides were thoroughly cleaned using acetone, isopropanol, and Milli-Q deionized water. After this, an LCs powder was applied to the surface of the glass. We set the nanocomposite sample thickness using spacers with a size of 50 μm . The working area of the electrodes in this structure was 1 cm². Next, the glass was heated to a temperature of 130°C. As a result of heating, the powder was melted and two glasses were connected, forming a sandwich cell.

To measure the electrical properties of the samples under study, we used a high-precision Sourcetronic ST2826A LCR Meter with a wide operating measurement range of frequencies from 20 Hz to 2 MHz. This allowed us to study the electrical parameters of the samples at different, widely spaced, frequencies. Impedance measurements were carried out with a peak amplitude of 0.25 V in the temperature range from 20°C to 130°C, allowing us to evaluate the influence of thermal factors on the electrical properties of the samples in different phase states. We used ultra-precise resistors and capacitances from the Vishay Precision Group to precisely calibrate the system and ensure high measurement accuracy. At each of the measured temperatures, we carried out at least three series of measurements in the frequency range from 20 Hz to 2 MHz. This provided us with more accurate and reliable data for calibration of the measurement setup. These data were used to analyze the electrical characteristics of the samples.

To automatize and simplify the measurement and data processing process, a special program was developed using Python script. This program not only allows us to carry out measurements for capacitance (C) and resistance (R) automatically but also to recalculate the values following our mathematical model of the sample, which included R and C connected in parallel. This significantly increased the efficiency and accuracy of our research. The overall measurement error is 1%-2%, which confirms the high reliability and quality of our results. To plot graphs of the dielectric constant, we used the following equations for real and imaginary parts:

$$\varepsilon' = \frac{Cd}{\varepsilon_0 S} \tag{1}$$

$$\varepsilon'' = \frac{d}{2\pi\varepsilon_0 f SR} \tag{2}$$

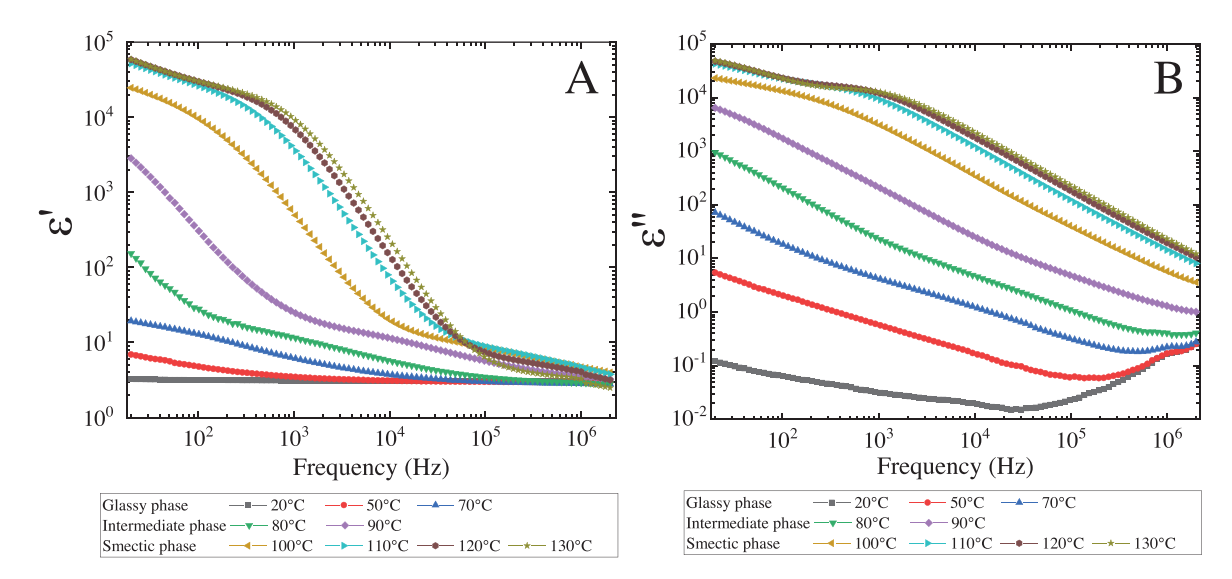


FIGURE 6 | Frequency dependencies of (A) the real part ε' and (B) imaginary part ε'' of the dielectric constant obtained for the CdC₈ at obtained different temperatures in the range from 20°C to 130°C for different phase states; glassy, intermediate and smectic.

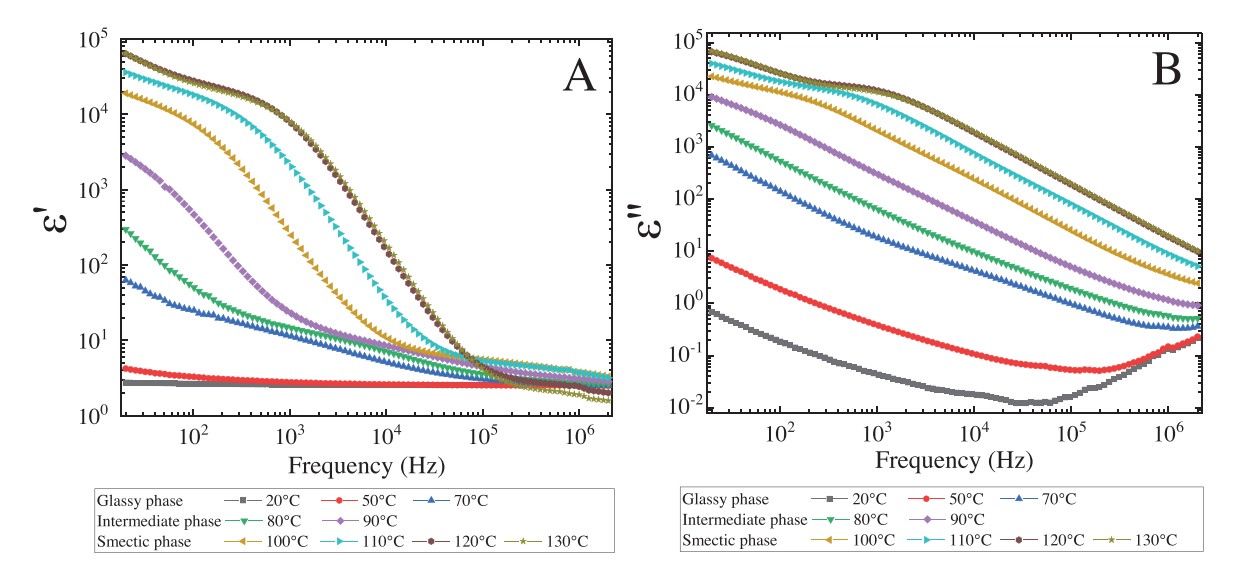


FIGURE 7 | Frequency dependencies of (A) the real part ε' and (B) imaginary part ε'' of the dielectric constant obtained for the CdC₈ + 2 wt% C obtained at different temperatures in the range from 20°C to 130°C for different phase states: glassy, intermediate, and smectic.

where C is the sample capacitance, d is the distance between the electrodes, ε_0 is the dielectric constant of the vacuum, S is the area of the electrodes, and R is the resistance of the sample.

An analysis of the real and imaginary parts of the dielectric constants is useful for understanding the electrical properties of the material, the material's response to the influence of electromagnetic fields, and the processes occurring inside the nanocomposite sample.

The analysis of data shown in Figures 6–9 reveals interesting effects. At low temperatures (below 90°C), the dependencies of ε' and ε'' on frequency show relatively stable behavior demonstrating the small deviation in real and imaginary parts as a function of frequency. However, when the temperature is increased above 100°C, noticeable changes in these parameters as a function of frequency are registered. The dielectric spectra were analyzed

more precisely for the temperature range \geq 100°C, corresponding to the smectic phase.

Experimental data showed that the components of the complex dielectric constant have large effective values in the smectic phase and change with increase of the temperature. The distribution of applied voltage along the structure changes with temperature. The applied voltage is distributed non-uniformly across the sample, with a significant voltage drop across thin near-electrode layers. These thin layers play an important role in the formation of the redistribution of electric field in the sample and affect the electrical properties of nanocomposite materials.

Figure 10 shows the Cole-Cole diagrams, where a certain part (shown by black, red, green, and blue half-circles) can be resolved, which can be described very well by a mathematical relationship.

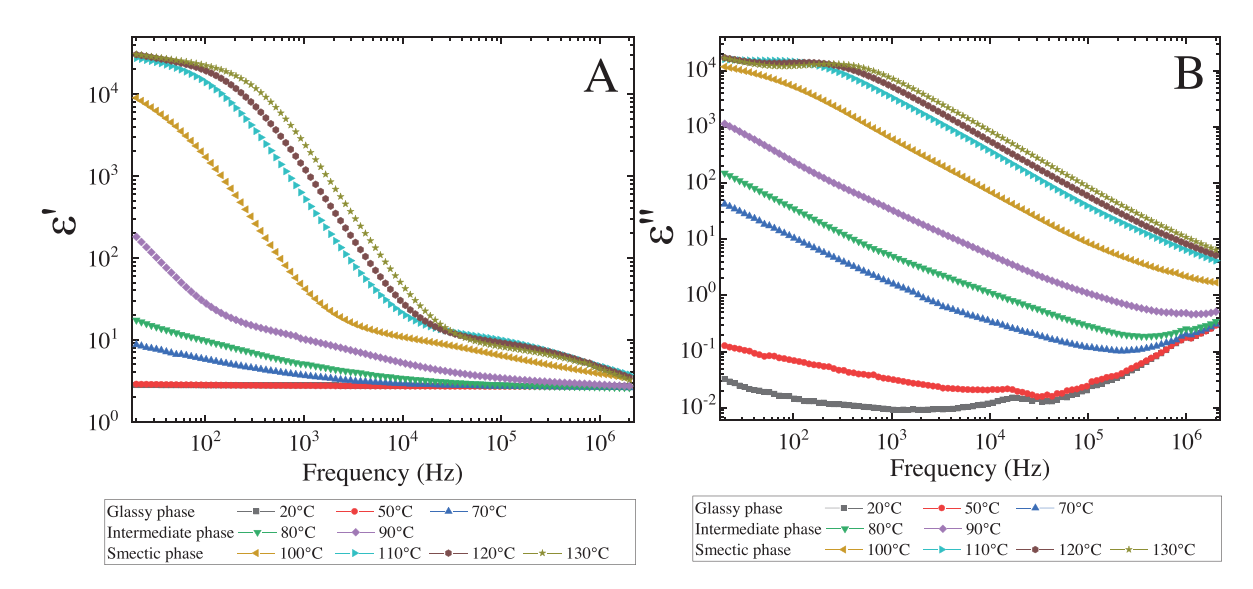


FIGURE 8 Frequency dependencies of (A) the real part ε' and (B) imaginary part ε'' of the dielectric constant obtained for the CdC₈ + 4 mol% Au obtained at different temperatures in the range from 20°C to 130°C for different phase states: glassy, intermediate and smectic.

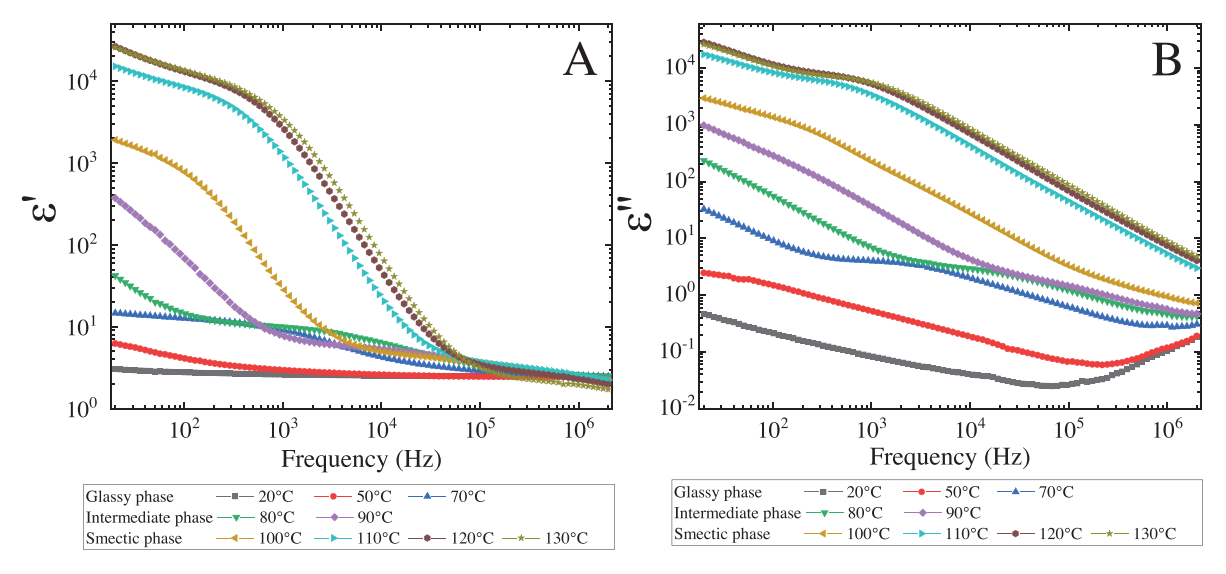


FIGURE 9 Frequency dependencies of (A) the real part ε' and (B) imaginary part ε'' of the dielectric constant obtained for the CdC₈ + 2 wt% C + 4 mol% Au obtained at different temperatures in the range from 20°C to 130°C for different phase states: glassy, intermediate, and smectic.

$$\frac{\varepsilon_s - \varepsilon_{\infty}}{\varepsilon^* - \varepsilon_{\infty}} = 1 + (i\omega\tau_{cc})^{1 - \alpha_{cc}}$$
(3)

 ε_{∞} is the value of the dielectric constant at $f=\infty$, ε_s is the value of the dielectric constant at f=0, ε^* is the complex dielectric constant of the material at a given temperature, ω is the frequency of the external electromagnetic field, τ_{cc} is the ColeCole relaxation time, α_{cc} is the ColeCole parameter (below in the text subscript cc will be omitted for simplicity).

This equation refers to the Debye dispersion modified by Cole-Cole and describes the behavior of the complex dielectric constant of a material as a function of frequency at high temperatures exceeding 100°C.

The study of the Cole-Cole diagrams and dielectric constant dispersion at different temperatures (100°C, 110°C, 120°C, and

130°C) allows us to understand how temperature changes influence the electrical properties of materials, and what charge transfer processes take place under different conditions. In this case, the initial part reflecting the high-frequency region of these diagrams is of interest. In the initial part of the Cole–Cole diagrams, a relaxation process is observed. The relaxation process can be caused by several polarization processes. In other words, it includes both free and bound charges. This process describes how quickly a material responds to high-frequency stimulation. The relaxation process in this context allows us to understand how quickly a material can adapt to changes in the electric field. These characteristics are important for understanding and using these materials in science and various technological applications.

However, as the frequency decreases, a change in the dielectric constant of the material is registered. In this case, the dispersion of the dielectric constant occurs. This low-frequency dispersion

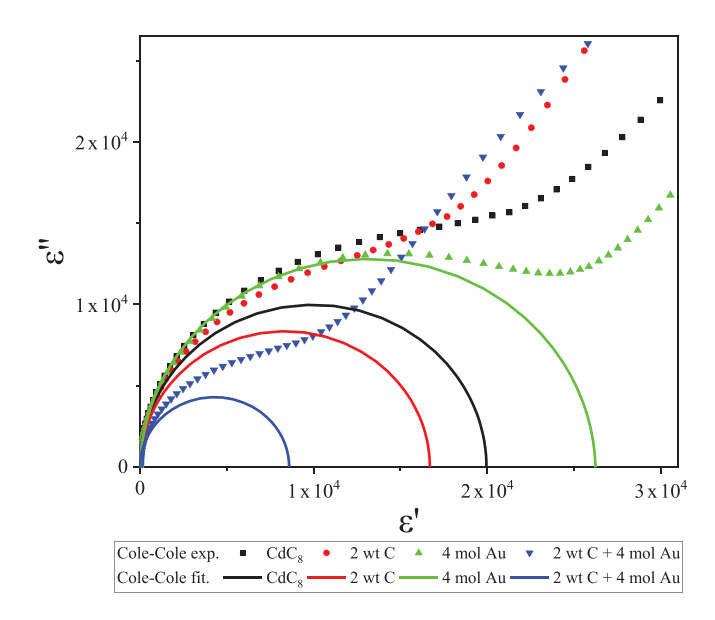


FIGURE 10 | Cole–Cole diagram obtained based on the frequency dependencies of ε' and ε'' for samples: CdC₈-black; CdC₈ + 2 wt% C-red; CdC₈ + 4 mol% Au–green; and CdC₈ + 2 wt% C + 4 mol% Au–blue at temperature 130°C.

is associated with the near-electrode processes. Charge transfer is determined by polarization processes near the electrode, that is, near the LC interface.

From the analysis of Cole–Cole diagrams, important parameters were obtained, such as relaxation times and the thicknesses of the near-electrode layer, in which the relaxation process occurs. In our structure, we have two electrodes; therefore, two near-electrode layers should be considered [34]. Then, the thickness of the near-electrode layer can be estimated using Equation (4) containing a coefficient equal to 2:

$$l_w = \frac{d}{2} \cdot \frac{\varepsilon_\infty}{\varepsilon_s} \tag{4}$$

 l_w is the thickness of the near-electrode region, in which the electrode polarization occurs, d is the distance between the electrodes, and ε_∞ is the value of dielectric constant at $f=\infty$, ε_s is the value of the dielectric constant at f=0. This formula allows us to estimate the thickness of the layer where the relaxation process occurs based on the extracted values of ε_s , ε_∞ and the distance between the electrodes. Let us consider in more detail the

parameters of relaxation processes, listed in Table 1, and obtained from the analysis of Cole–Cole diagrams for each of the presented series of samples:

Using slopes obtained from graphs in Arrhenius coordinates shown in Figure 11, we can calculate the conduction activation energy for each of materials using the following relation:

$$\sigma = \sigma_{0i} \, \exp\left(-\frac{E_{ai}}{k_B T}\right) \tag{5}$$

where σ_{0i} is the parameter, depending on ionic phase of LC, E_{ai} is the activation energy of ionic conduction, E_{ae} and k_B is the Boltzmann constant.

The energies are listed in Table 2. The data show that introduced NPs result in changes of the relaxation time and in turn in change of the activation energy. In a smectic phase, it increases from 0.44 (CdC₈) to 0.56 eV (CdC₈ + 2 wt% C) and 0.62 eV (CdC₈ + 4 mol% Au). It should be emphasized that when two types of NPs (i.e., both C and Au) were added to an LC matrix, a decrease in the activation energy was detected (from 0.44 to 0.37 eV). This change in sign was also observed in a nonlinear-optical experiment performed using the same materials [35], and possible interactions between C and Au NPs were suggested as an explanation. A decrease in the activation energy instead of its increase of the activation energy of the relaxation time in our experiment reflecting transport properties can be explained by the increase in concentration of charge carriers along cation-anion layers in the nanocomposite material containing C and Au NPs.

The relaxation time strongly depends on the sample composition (synthesis of C and Au NPs) and temperature. The introduced NPs, as well as temperature changes, significantly affect the relaxation rate. Samples with the addition of C and Au NPs have longer relaxation times, which may indicate a change in the structure of the material. The thickness of the near-electrode layer also varies depending on the sample composition and temperature. Samples with the addition of Au NPs have a thicker near-electrode layer, which is associated with a change in the structural composition of the material. The coefficient α —statistical distribution of relaxation times, remains almost unchanged with changes in the composition of the samples, but it varies slightly with temperature.

TABLE 1 Parameters of relaxation processes of samples: CdC₈, CdC₈ + 2 wt% C, CdC₈ + 4 mol% Au, CdC₈ + 4 mol% Au + 2 wt% C depending on temperature, *T*.

	CdC ₈ Matrix			CdC ₈ + 2 wt% C		CdC ₈ + 4 mol% Au		CdC ₈ + 4 mol% Au + 2 wt% C				
T,°C	τ , ms ^a	l, nm	$1-\alpha^{\mathbf{b}}$	τ, ms ^a	l, nm	$1-\alpha^{\mathbf{b}}$	τ, ms ^a	<i>l</i> , nm	$1-\alpha^{\mathbf{b}}$	τ, ms ^a	l, nm	$1-\alpha^{b}$
100	1.25	6.4	0.96	1.43	6.6	1	4.50	9.6	0.95	1.90	35	0.94
110	0.31	6.6	1	0.37	7.3	1	1.36	5.0	0.97	0.33	9.6	1
120	0.21	4.6	1	0.23	2.9	1	0.82	4.7	0.97	0.24	6.3	1
130	0.16	3.5	1	0.16	2.5	1	0.53	4.2	0.98	0.19	5.4	1

^aAverage value of 95% confidence interval of parameter $\tau_{matrix} \approx 3.1 \times 10^{-4}$ ms, $\tau_c \approx 4.2 \times 10^{-4}$ ms, $\tau_{au} \approx 1.6 \times 10^{-3}$ ms, $\tau_{c+au} \approx 6.5 \times 10^{-4}$ ms.

^b Average value of 95% confidence interval of parameter $1 - \alpha_{matrix} \approx 1.3 \times 10^{-4}, 1 - \alpha_{c} \approx 1.3 \times 10^{-4}, 1 - \alpha_{au} \approx 1.8 \times 10^{-5}, 1 - \alpha_{c+au} \approx 1.4 \times 10^{-4}$.

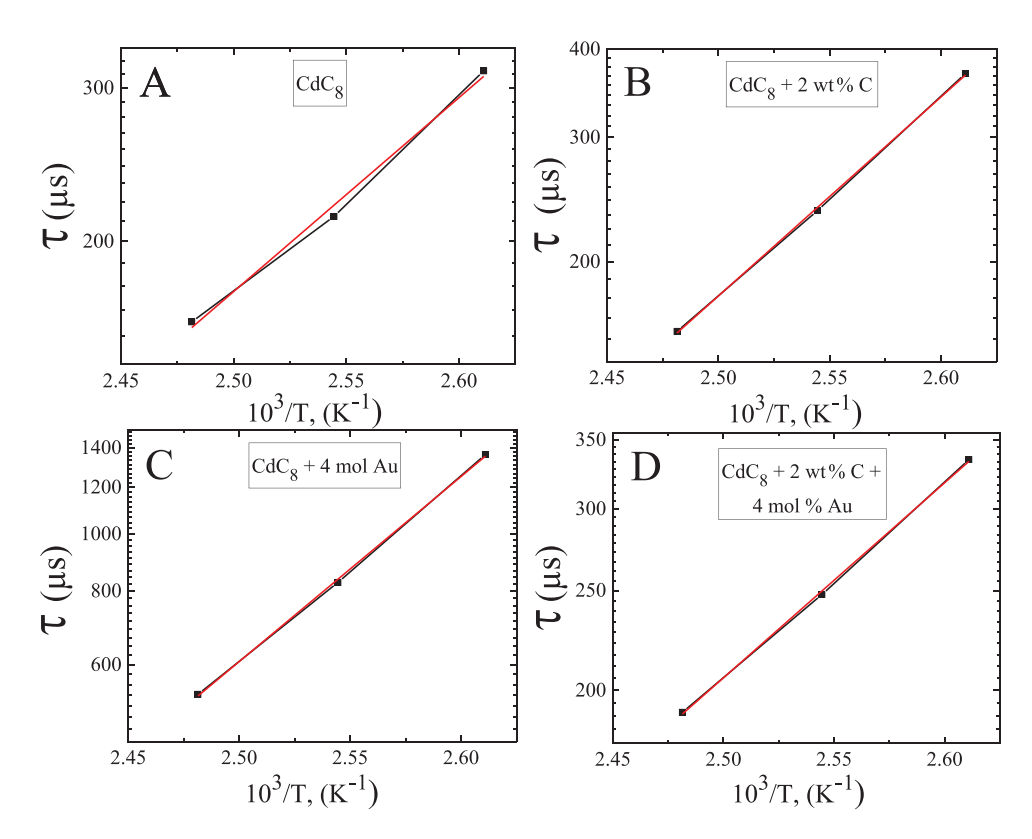


FIGURE 11 Relaxation time versus inverse temperature for: (A) CdC₈, (B) CdC₈ + 2 wt% C, (C) CdC₈ + 4 mol% Au, and (D) CdC₈ + 2 wt% C + 4 mol% Au at different temperatures (110°C, 120°C, 130°C). Black lines—experimental data; red lines—the fitting of the experimental data.

The conductivity of the material can also be calculated from the data obtained using the following equation:

$$\sigma = \frac{d}{R} \cdot \frac{1}{S} = 2\pi \varepsilon_0 f \varepsilon'' \tag{6}$$

The data in Figure 12 show that with an increasing concentration of NPs, the conductivity of the material decreases at all temperatures and for all samples. This can be explained by the following considerations. NPs can introduce additional traps into the crystal structure of the material, which leads to a decrease in conductivity. In addition, NPs in an LC phase can capture ions, effectively immobilizing them and leading to a decrease in the electrical conductivity [36].

It should be noted that as the temperature increases, the conductivity of all samples also increases because of the decrease in the viscosity of samples and the corresponding increase in the charge mobility. In addition, there is a series of phase transitions leading to changes in the morphology of the studied samples. All studied samples are in a glass phase at room temperature. As the temperature keeps increasing, a glassy state turns into an LC phase at a temperature of about 100°C. As a result, the electrical conductivity increases as the temperature increases.

The measured dielectric spectra also allowed to evaluate the electrical properties of the studied samples. According to Figures 6–9, the glassy phase, intermediate phase, and smectic phase exhibit different types of frequency dependence on the imaginary part of the dielectric constant. To account for this fact, the electrical conductivity was evaluated at two frequencies: 10 kHz (Figure 12A) and 1 MHz (Figure 12B). By plotting graphs in Arrhenius coordinates, we estimated the activation energy of the electrical conductivity for the studied samples. Arrhenius coordinates represent the inverse temperature (1/T) on the horizontal axis and the logarithm of conductivity ($\ln[\sigma]$) on the vertical axis. This representation allows us to analyze the temperature dependence of conductivity to obtain the activation energy.

From the graphs in Arrhenius coordinates in Figures 13 and 14, we can calculate the conduction activation energy, which is the energy required for charge carriers to cross the energy barrier.

In general, we can assume two dominant types of charge carriers: electrons and ions, and apply the following equation:

$$\sigma = \sigma_{0i} \exp\left(-\frac{E_{ai}}{k_B T}\right) + \sigma_{0e} \exp\left(-\frac{E_{ae}}{k_B T}\right)$$
 (7)

TABLE 2 | The activation energy of the relaxation time for the studied samples in a smectic phase.

Sample	CdC ₈	2 wt% C	4 mol% Au	2 wt% C + 4 mol% Au
E_a (eV)	0.44	0.56	0.62	0.37

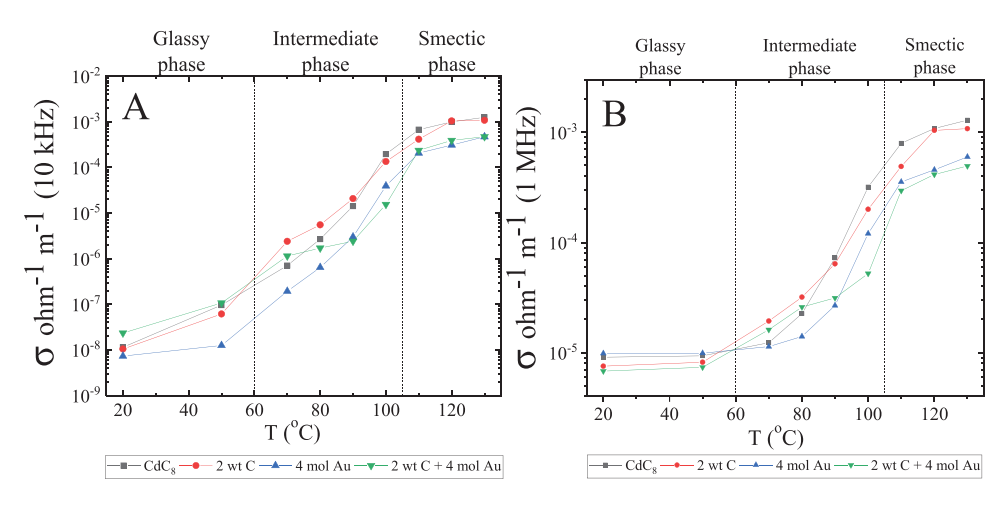


FIGURE 12 Conductivity for the studied samples, obtained at different temperatures and NPs concentrations (CdC_8 , $CdC_8 + 4$ mol% Au, $CdC_8 + 2$ wt% C, $CdC_8 + 4$ mol% Au + 2 wt% C) from measured data at frequency (A) 10 kHz and (B) 1 MHz.

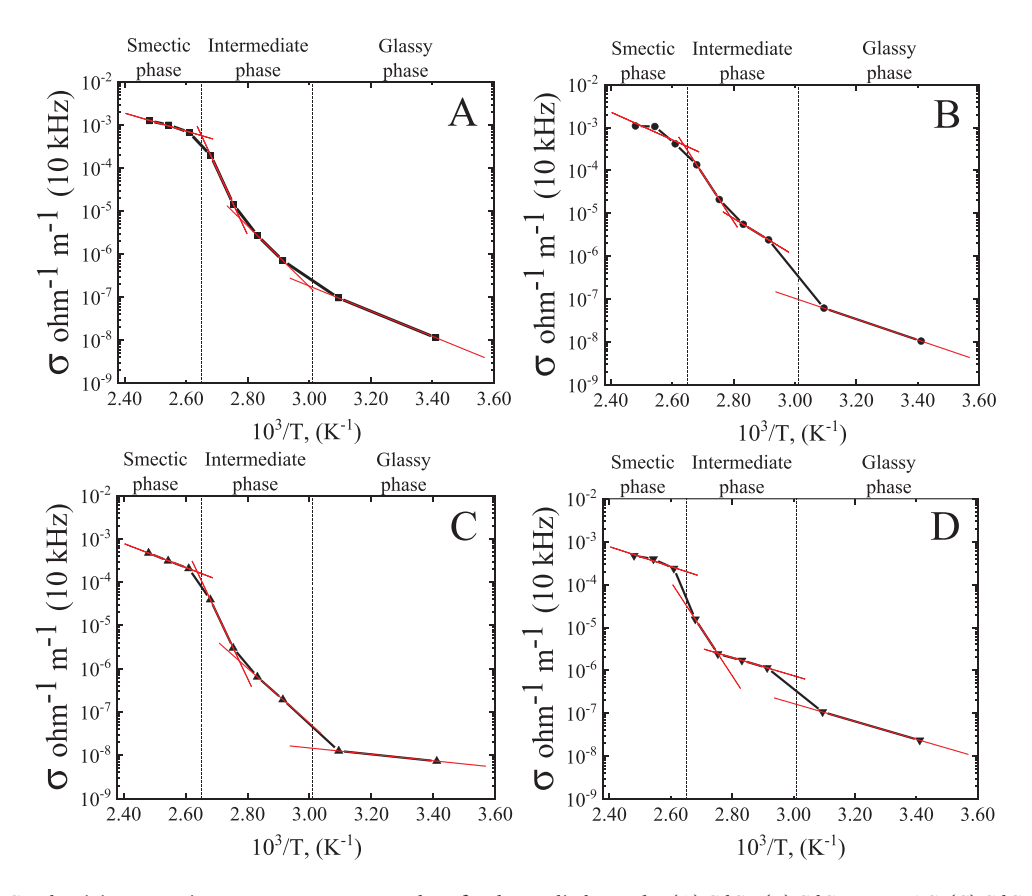


FIGURE 13 Conductivity versus inverse temperature at 10 kHz for the studied samples (A) CdC_8 , (B) $CdC_8 + 2$ wt% C, (C) $CdC_8 + 4$ mol% Au and (D) $CdC_8 + 2$ wt% C + 4 mol Au at different temperatures obtained from measured data at 10 kHz and different temperatures. Black lines—experimental data, red lines—the fitting of the experimental data.

where σ_{0e} is the parameter, depending on electronic phase of LC, E_{ae} is the activation energy of electronic conduction.

The data of Figures 13 and 14 can be used to analyze three different states of the material: the glass phase, the intermediate phase, that is, supercooled liquid crystalline state (where the LC gradually changes from the glass phase to the smectic phase), and the smectic phase [30]. The activation energy

of conductivity, which characterizes the ability of a material to conduct electricity as temperature changes, depends on the type of NPs (i.e., Au, C, or the combination of Au and C NPs). According to Figures 13 and 14 and Tables 3 and 4, the activation energy of the conductivity for all studied samples shows a qualitatively similar trend. At the same time, the addition of NPs results in noticeable quantitative changes.

26884011, 2025, 8, Down

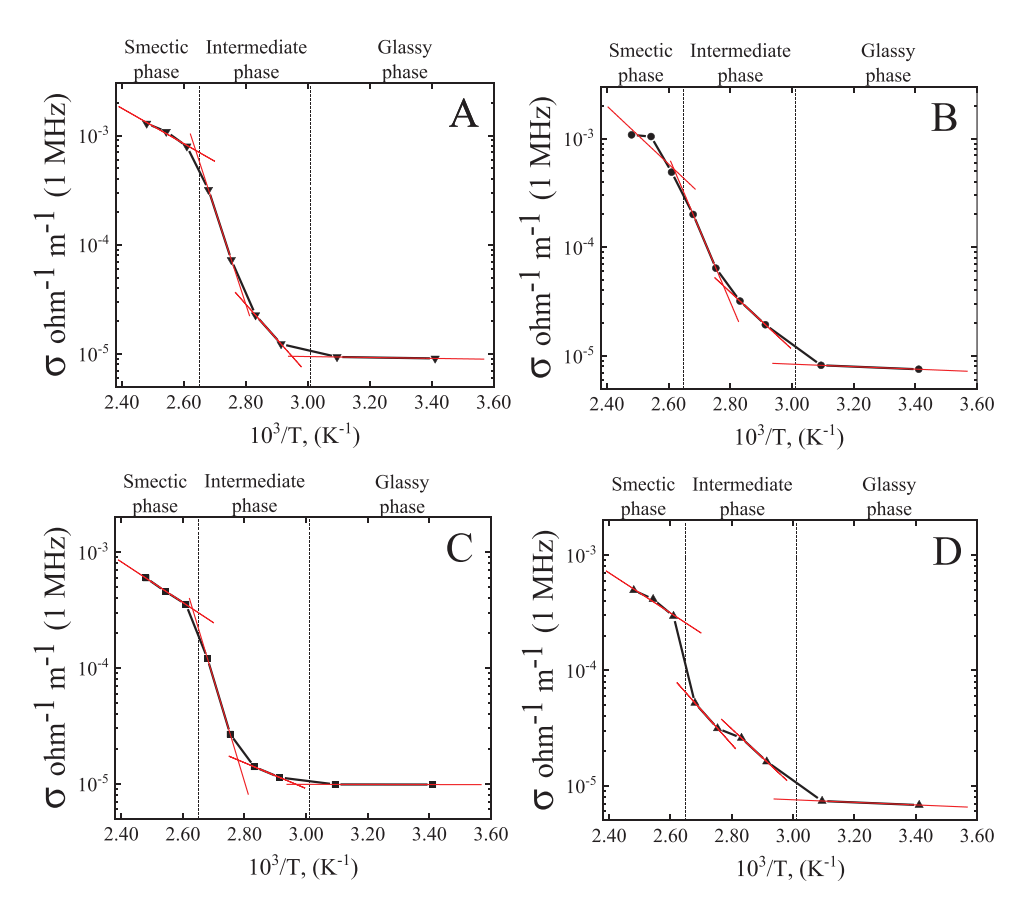


FIGURE 14 Conductivity versus inverse temperature at 1 MHz for the studied samples (A) CdC_8 , (B) $CdC_8 + 2$ wt% C, (C) $CdC_8 + 4$ mol% Au, and (D) $CdC_8 + 2$ wt% C + 4 mol Au at different temperatures obtained from measured data at 1 MHz and different temperatures. Black lines—experimental data; red lines—the fitting of the experimental data.

TABLE 3 | Activation energy of conductivity in different phases at 10 kHz for several nanocomposite materials.

Sample	CdC ₈	2 wt% C	4 mol% Au	2 wt% C + 4 mol% Au
E_a (eV) in glass	0.5793	0.4808	0.1470	0.4133
E_{ae} (eV)	1.3954	0.8700	1.2589	0.4204
E_{ai} (eV)	2.0715	2.1820	3.0061	2.1735
E_a (eV) in smectic	0.4155	0.6407	0.5480	0.4601

TABLE 4 | Activation energy of conductivity in different phases at 1 MHz for several nanocomposite materials.

Sample	CdC ₈	2 wt% C	4 mol% Au	2 wt% C + 4 mol% Au
E_a (eV) in glass	0.0082	0.0228	0.0007	0.0221
E_{ae} (eV)	0.6355	0.5232	0.2213	0.4937
E_{ai} (eV)	1.7312	1.3316	1.7564	0.5949
E_a (eV) in smectic	0.3211	0.5307	0.3482	0.3452

Estimated activation energy from conductivity versus temperature in different phases at 10 kHz is listed in Table 3 for the following nanocomposite materials: CdC_8 matrix, CdC_8+4 mol% Au, CdC_8+2 wt% C, CdC_8+4 mol% Au +2 wt% C.

For all three phases, the activation energy of conductivity was calculated (Table 4), which allows us to investigate in more detail the changes in the structure and conductivity of the material upon the introduction of C and Au NPs.

Glass phase. We analyzed data for the glass phase. The matrix is characterized by a low conduction activation energy (0.5793 eV for 10 kHz and 0.0082 eV for 1 MHz), which indicates that in this phase, charge transport takes place relatively easily. It can be explained by assuming electronic charge carriers and considering an LC glassy phase facilitating electronic transport. When Au NPs are added, the activation energy decreases from 0.5793 to 0.1470 eV for 10 kHz and from 0.0082 to 0.0007 eV for 1 MHz. This reflects that Au NPs assist in increasing the conductivity of the material in the glass phase. Au NPs can be good electronic conductors, and their presence facilitates the transport of electrons. The inclusion of C reduces the conduction activation energy to 0.4808 eV for the 10 kHz range and increases the activation energy of conduction to 0.0228 eV for 1 MHz. When C is introduced into the material, the movement of electrons behaves differently depending on the frequency; for 10 kHz, conduction activation energy decreases, which increases the conductivity, and conversely for 1 MHz, conduction activation energy increases and conductivity decreases. The combined introduction of C and Au NPs also depends on the measurement frequency and is similar to the behavior in the addition of C NPs

Intermediate phase. The intermediate phase, which occurs in the temperature range of approximately 60°C-100°C between the smectic A and glassy phases, specifically between the melting temperature, and the glass transition temperature is a supercooled smectic liquid. In this state, as the temperature increases, the material softens and its viscosity decreases. In this intermediate range, we considered two types of dominant charge carriers of electronic (70°C to 80°C) and ionic (90°C to 100°C) origin. The incorporation of C and Au NPs to the matrix CdC₈ reduces the activation energy of electronic conduction for the intermediate phase from 1.3954 to 0.4204 eV for 10 kHz and from 0.6355 to 0.2213 eV for 1 MHz. This reflects that C and Au NPs improve the electronic conductivity of the material, making it more efficient at conducting electricity. As for the activation energy of ionic conductivity for the intermediate phase when adding Au and C NPs, the samples behave differently for 10 kHz and 1 MHz. At 10 kHz the addition of NPs results in an increase in the activation energy of the ionic conductivity. This can be explained by additional energy barriers created by NPs on the path of ionic charge carriers. As a result, NPs inhibit the process of ionic transport, which is reflected by larger values of the activation energy of the ionic conductivity. It should be noted that the electrical conductivity measured at 10 kHz can be associated with direct current (DC) conductivity mostly whereas the electrical conductivity measured at 1 MHz has a dominant contribution due to alternating current (AC) conductivity, which can explain the difference in the values of the activation energies listed in Tables 3 and 4.

Smectic phase. At approximately 100°C, we registered a phase transition from the intermediate phase to the smectic A phase. The smectic A phase is the ordered structure of the material. In this phase, the material has a high degree of order, and the charge transfer occurs mostly by ions. A study of the smectic A phase of the material showed that C and Au NPs can slightly increase the activation energy from 0.4155 to 0.6407 eV for 10 kHz and from 0.3211 to 0.5307 eV for 1 MHz. This can be explained by considering that in the smectic A phase, charges are transferred

mainly by ions, and the presence of NPs can result in disorder in the smectic structure and act as additional scattering centers for the transfer of charge carriers.

5 | Conclusion

SEM and TEM results demonstrate that C NPs introduced into the matrix of nanocomposite material have a size distribution in the range of 5-9 nm, and Au NPs in the nanocomposite material have average diameters of 15-20 nm. The characteristic sizes of NPs show a small dispersion. The relaxation time, the thickness of the layer adjacent to the electrode layer, and the α coefficient of materials with the inclusion of C and Au NPs depend on the sample composition and temperature. The synthesis of C and Au NPs has a significant effect on the relaxation rate, reflecting a change in the structure of the material. The addition of Au NPs leads to an increase in the thickness of the near-electrode layers, which is associated with structural changes impacting the near-electrode regions of the sample. C and Au NPs reduce the conductivity of the matrix, and this phenomenon strongly depends on temperature. Factors inhibiting the electrical conductivity of the studied samples include the formation of additional scattering centers on the path of charge carriers and the capturing of ionic charge carriers by NPs. The experimental results suggest the presence of two major charge carriers of electronic and ionic origins. Electrons are the main charge carriers in the glassy phase; however, ions become dominant charge carriers in the intermediate phase and smectic phase. The electrical conductivity of all samples increases with the temperature rise, thus exhibiting Arrhenius-like behavior. The results reveal that nanocomposite materials have three different states: glass phase, intermediate phase, and smectic phase. In all three phases, more clearly in the smectic A phase, an addition of NPs results in a decrease in the conductivity of carriers that move perpendicular to the cation-anion layers. These results highlight the importance of composition and temperature control to achieve specific material performance for a variety of applications. These nanocomposites exhibit a variety of unique characteristics and have great potential in a wide range of scientific fields, including nanotechnology and the design of new materials.

Acknowledgments

D. Zhulai greatly appreciates a research grant from the German National Academy of Sciences Leopoldina. Y. Garbovskiy would like to acknowledge funding from the CSU—AAUP Faculty Research Grant and the NASA CT Space Grant. The authors acknowledge funding from NASU via the project No. 0123U100832.

Open Access funding enabled and organized by Projekt DEAL.

Conflicts of Interest

The authors declare no conflicts of interest.

Data Availability Statement

The data that support the findings of this study are available from the corresponding author upon reasonable request.

References

- 1. A. Facchetti, "Made to Order: Organic Semiconductors," *Nature Materials* 12 (2013): 598–600.
- 2. A. J. J. M. Van Breemen, P. T. Herwig, C. H. T. Chlon, et al., "Large Area Liquid Crystal Monodomain Field-Effect Transistors," *Journal of the American Chemical Society* 128, no. 7 (2006): 2336–2345.
- 3. H. K. Park, K. E. Schriver, and R. F. Haglund, "Resonant Infrared Laser Deposition of Polymer-Nanocomposite Materials for Optoelectronic Applications," *Applied Physics A Material Science and Processing* 105 (2011): 583–592.
- 4. C. Lu, H.-C. Chen, W.-T. Chuang, Y.-H. Hsu, W.-C. Chen, and P.-T. Chou, "Interplay of Molecular Orientation, Film Formation, and Optoelectronic Properties on Isoindigo- and Thienoisoindigo-Based Copolymers for Organic Field Effect Transistor and Organic Photovoltaic Applications," *Chemistry of Materials* 27, no. 19 (2015): 6837–6847.
- 5. H. Grohganz, K. Löbmann, P. Priemel, et al., "Amorphous Drugs and Dosage Forms," *Journal of Drug Delivery Sciences and Technology* 23, no. 4 (2013): 403–408.
- 6. S. K. Murthy, "Nanoparticles in Modern Medicine: State of the Art and Future Challenges," *International Journal of Nanomedicine* 2, no. 2 (2007): 129–141.
- 7. S. Chen, Q. Zhang, Y. Hou, J. Zhang, and X.-J. Liang, "Nanomaterials in Medicine and Pharmaceuticals: Nanoscale Materials Developed With Less Toxicity and More Efficacy," *European Journal of Nanomedicine* 5, no. 2 (2013): 61–79.
- 8. A. Yetisgin, S Cetinel, M. Zuvin, A. Kosar, and O. Kutlu, "Therapeutic Nanoparticles and Their Targeted Delivery Applications," *Molecules* 25, no. 9 (2020): 2193.
- 9. T. M. Joseph, D. Kar Mahapatra, A. Esmaeili, et al., "Nanoparticles: Taking a Unique Position in Medicine," *Nanomaterials* 13 (2023): 574.
- 10. J. K. Patra, G. Das, and L. F. Fraceto, "Nano Based Drug Delivery Systems: Recent Developments and Future Prospects," *Journal of Nanbiotechnology* 16 (2018): 71.
- 11. Y. K. Mishra, S. Mohapatra, D. Kabiraj, et al., "Synthesis and Characterization of Ag Nanoparticles in Silica Matrix by Atom Beam Sputtering," *Scripta Materialia* 56, no. 7 (2007): 629–632.
- 12. A. Bukowczan, E. Hebda, and K. Pielichowski, "The Influence of Nanoparticles on Phase Formation and Stability of Liquid Crystals and Liquid Crystalline Polymers," *Journal of Molecular Liquids* 321 (2021): 114849.
- 13. T. Hegmann, H. Qi, and V. M. Marx, "Nanoparticles in Liquid Crystals: Synthesis, Self-Assembly, Defect Formation and Potential Applications," *Journal of Inorganic and Organometallic Polymers and Materials* 17 (2007): 483–508.
- 14. M. Rahimi, T. F. Roberts, J. C. Armas-Pérez, et al., "Nanoparticle Self-Assembly at the Interface of Liquid Crystal Droplets," *Applied Physical Sciences* 112, no. 17 (2015): 5297–5302.
- 15. Y. Yan, J. Gong, J. Chen, et al., "Recent Advances on Graphene Quantum Dots: From Chemistry and Physics to Applications," *Advanced Materials* 31 (2019): 1808283.
- 16. J. Liu, R. Li, and B. Yang, "Carbon Dots: New Type of Carbon-Based Nanomaterial With Wide Applications," *ACS Central Science* 6, no. 12 (2020): 2179–2195.
- 17. I. Khan, K. Saeed, and I. Khan, "Nanoparticles: Properties, Applications and Toxicities," *Arabian Journal of Chemistry* 12, no. 7 (2019): 908–931.
- 18. K. Goossens, K. Lava, C. W. Bielawski, and K. Binnemans, "Ionic Liquid Crystals: Versatile Materials," *Chemical Reviews* 116, no. 8 (2016): 4643–4807.
- Q. Ruan, M. Yao, D.u Yuan, et al., "Ionic Liquid Crystal Electrolytes: Fundamental, Applications and Prospects," Nano Energy 106 (2023): 108087

- 20. S. J. Devaki and R. Sasi, *Ionic Liquids/Ionic Liquid Crystals for Safe and Sustainable Energy Storage Systems* (London, UK: In Tech Open, 2017).
- 21. N. Kapernaum, A. Lange, M. Ebert, et al., "Current Topics in Ionic Liquid Crystals," *ChemPlusChem* 87, no. 1 (2021): e202100397.
- 22. K. Binnemans, "Ionic Liquid Crystals," *Chemical Reviews* 105, no. 11 (2005): 4148–4204.
- 23. D. Zhulai, S. Bugaychuk, G. Klimusheva, et al., "Structural Characteristics of Different Types of Nanoparticles Synthesized in Mesomorphic Metal Alkanoates," *Liquid Crystals* 44, no. 8 (2017): 1269–1276.
- 24. V. Rudenko, A. Tolochko, D. Zhulai, et al., "Intensity-dependent Optical Nonlinearities of Composite Materials Made of Ionic Liquid Crystal Glass and Bimetallic Nanoparticles," *Liquid Crystals* 50, no. 1 (2022): 174–180.
- 25. V. Rudenko, A. Tolochko, S. Bugaychuk, et al., "Exploring Optical Nonlinearities of Glass Nanocomposites Made of Bimetallic Nanoparticles and Mesogenic Metal Alkanoates," *Materials Proceedings* 14, no. 1 (2023): 19.
- 26. V. Rudenko, A. Tolochko, S. Bugaychuk, et al., "Probing Optical Nonlinearities of Unconventional Glass Nanocomposites Made of Ionic Liquid Crystals and Bimetallic Nanoparticles," *Nanomaterials* 12 (2022): 924.
- 27. D. Zhulai, O. Kovalchuk, S. Bugaychuk, G. Klimusheva, T. Mirnaya, and S. Vitusevich, "Photovoltaic Properties of cd-based Ionic Liquid Crystals With Semiconductor Nanoparticles," *Molecular Crystals and Liquid Crystals* 750, no. 1 (2023): 32–41.
- 28. D. Zhulai, O. Kovalchuk, S. Bugaychuk, G. Klimusheva, T. Mirnaya, and S. Vitusevich, "Photoconductivity of Ionic Thermotropic Liquid Crystal With Semiconductor Nanoparticles," *Journal of Molecular Liquids* 267 (2018): 406–410.
- 29. T. A. Mirnaya, S. V. Volkov, I.n: R. D. Rogers, K. R. Seddon, and S. V. Volkov, "Green Industrial Applications of Ionic Liquids," *NATO Science Series II (Mathematics, Physics and Chemistry)* 92 (2002): 439–456.
- 30. V. N. Asaula, T. A. Mirnaya, G. G. Yaremchuk, and A. S. Tolochko, "Mesomorphic and Glass-forming Properties of the Homologous Series of Cadmium Alkanoates," *Ukrainian Chemistry Journal* 77, no. 1 (2011): 24–27.
- 31. V. M. Ogenko, L. B. Kharkova, O. G. Yanko, S. I. Orysik, and E. M. Mashkova: The Method of Synthesis of Carbon Quantum Dots, Ukrainian Patent N 2021 00294 (2021).
- 32. T. A. Mirnaya, G. G. Yaremchuk, N. A. Leonova, et al.: Process for Preparation of Liquid Crystal Nanocomposite Materials With Gold Nanoparticles, Ukrainian Patent UA86660, (2014).
- 33. D. Zhulai, D. Fedorenko, O. Kovalchuk, S. Bugaychuk, G. Klimusheva, and T. Mirnaya, "Influence of Semiconductor and Metal Nanoparticles on the Dielectric Properties of Ionic Matrix Cadmium Octanoate," *Nanoscale Research Letters* 10, no. 1 (2015): 66.
- 34. T. M. W. J. Bandara and B. E. Mellander, "Evaluation of Mobility, Diffusion Coefficient and Density of Charge Carriers in Ionic Liquids and Novel Electrolytes Based on a New Model for Dielectric Response," in *Ionic Liquids: Theory, Properties, New Approaches*, eds. T. M. W. J. Bandara and B.-E. Mellander (London, UK: In Tech, 2011), 383–408.
- 35. V. Rudenko, A. Tolochko, S. Bugaychuk, et al., "Modifying Optical Nonlinearities of Ionic Liquid Crystal Glass by Adding Gold and Carbon Nanoparticles," *Journal of Molecular Liquids* 393 (2024): 123641.
- 36. Y. Garbovskiy, "Conventional and Unconventional Ionic Phenomena in Tunable Soft Materials Made of Liquid Crystals and Nano-Particles," *Nano Express* 2 (2021): 012004.